Inkjet printing multi-deposited YBCO on $CGO/LMO/MgO/Y_2O_3/Al_2O_3$/Hastelloy tape for 2G Coated Conductors

Valentina Roxana Vlad, Elena Bartolomé, Marta Vilardell, Albert Calleja, Alexander Meledin, Xavier Obradors, Teresa Puig, Susagna Ricart, Gustaaf Van Tendeloo, Alexander Usoskin, Sergey Lee, Valery Petrykin, and Alexander Molodyk

***Abstract*—We present the preparation of a new architecture of coated conductor by Inkjet printing of low fluorine $YBa_2Cu_3O_{7-x}$ (YBCO) on top of SuperOx tape: $CGO/LMO/IBAD\text{-}MgO/Y_2O_3/Al_2O_3$/Hastelloy. A 5-layered multi-deposited, 475 nm thick YBCO film was structurally and magnetically characterized. A good texture was achieved using this combination of buffer layers, requiring only a 30 nm thin IBAD-MgO layer. The LF-YBCO CC reaches self-field critical current density values of J_c^{GB}~15.9 MA/cm^2 (5 K), ~1.23 MA/cm^2 (77 K) corresponding to an I_c(77K)=58.4 A/cm-width. Inkjet printing offers a flexible and cost effective method for YBCO deposition, allowing patterning of structures.**

Index Terms—Coated Conductors, Inkjet printing,

I. Introduction

NOWADAYS, 2G CCs have demonstrated their high utility for generation, transport and storage of energy applications at liquid nitrogen temperatures [1]. Chemical Solution Deposition (CSD) of YBCO is considered the most cost-effective, efficient scalable method to cover the needs of the CC superconducting market. *Slot-die coating* has been used by D-Nano (Germany) to achieve CCs with record I_c=300 A/cm-width (77 K) in Europe, within the Eurotapes project [2]. *Inkjet printing* is another technique, which allows the deposition of different oxides through the use of chemical inks [3],[4]. Inkjet deposition of YBCO films from low-fluorine (LF) precursor solutions has been reported [5]. An advantage of Inkjet printing is that it permits patterning structures. Stripes of YBCO for AC-losses reduction have been successfully prepared on both RABiTs (Rolling-Assisted Biaxially Textured Substrates) [6] and ABAD (Alternating Beam Assisted Deposition) [7],[8] CC architectures. The ABAD method enables the use of a polycrystalline substrate, however it must be textured through a thick layer (> 1µm) of YSZ [9]. In the architecture presented in this paper, a 30 nm layer of MgO prepared by ion-beam-assisted deposition (IBAD) is enough to achieve a good texture, comparable to IBAD-YSZ variants.

II. Experimental

A. Sample Fabrication

A new 2G CC architecture was prepared at Oxolutia, based on the CSD multi-deposition by Inkjet printing of YBCO on top of the tape provided by SuperOx: $YBa_2Cu_3O_{7-x}$/CGO/LMO/IBAD-MgO/Y_2O_3/Al_2O_3/Hastelloy.

SuperOx tape consists of a 60 µm-thick Hastelloy C276 metallic substrate covered by various vacuum-deposited buffer layers which are used to transfer the texture to YBCO and adjust the lattice parameters: a sputtered Al_2O_3 (70 nm), RF-sputtered Y_2O_3 (10 nm), IBAD MgO (30 nm), RF-sputtered $LaMnO_3$ (LMO) (30 nm) and a PLD Gd:CeO_2 (CGO) (200 nm) layer [10].

The YBCO chemical solution is deposited on top of this substrate by reel-to-reel Inkjet printing multinozzle deposition. In this work, the YBCO layer was prepared using a low-fluorine YBCO solution, thanks to which the quantity of fluorine was decreased 80% compared to the pure TFA-solution, and the processing time was reduced [11]. The LF YBCO solution (0.5 M) is

This work was performed within the framework of the EUROTAPES project (FP7-NMP.2011.2.2-1 Grant no. 280432), funded by the EU. ICMAB research was financed by the Ministry of Economy and Competitiveness, and FEDER funds under projects MAT2011-28874-C02-01, MAT2014-51778-C2-1-R, ENE2014-56109-C3-3-R and Consolider Nanoselect CSD2007-00041, and by Generalitat de Catalunya (2009 SGR 770, 2015 SGR 753 and Xarmae). ICMAB acknowledges support from Severo Ochoa Program (MINECO, Grant SEV-2015-0496). *(Corresponding author: Valentina Roxana Vlad)*

V.R. Vlad, A. Calleja and M. Vilardell are with Oxolutia SL, 08210, Barberà del Vallès, Spain (e-mail: vrvlad@oxolutia.com).

E. Bartolomé is with Escola Universitària Salesiana de Sarrià (EUSS), Barcelona, Spain

A. Medelin and G. Van Tendeloo are with Electron microscopy for Materials Science (EMAT), Physics Dep., Antwerp University, Belgium

T. Puig, S. Ricart and X. Obradors are with the Institut de Ciència de Materials de Barcelona (ICMAB-CSIC), 08193 Bellaterra, Spain

A. Usoskin is with Bruker HTS GmbH , D-63755 Alzenau, Germany

A. Molodyk is with ZAO SuperOx, Moscow 117246, Russia

S. Lee and V. Petrykin is with SuperOx Japan LLC, Kamimizo, 252-0243 Japan

obtained by mixing yttrium trifluoroacetate (TFA) with barium 2-ethylhexanoate and copper acetate in a highly boiling point solvent. After the YBCO deposition, the CC tape is subjected to a thermal process consisting of pyrolysis, growth and oxygenation [12]. Thicker YBCO layers can be achieved by multi-deposition.

In this work we present the structural and magnetic characterization of an optimized CC, with a superconducting YBCO film of 475±25 nm thickness achieved by 5-cycles of multi-deposition (sample LF-YBCO). The superconducting performance of this sample is compared with that of a previously characterized CC also prepared by Inkjet printing, but starting from a 0.5M TFA solution and with a different architecture: TFA-$YBa_2Cu_3O_{7-x}$/CZO/ABAD-YSZ/SS [4]. This t=0.9 μm thickness film was obtained after the growth of three cycles of deposition-pyrolysis, and is denoted as TFA-YBCO.

B. Experimental details

The YBCO deposition has been performed using an in-house built inkjet printer using a Konica Minolta piezoelectric printhead with 512 nozzles. The structural characterization by X-ray diffraction was done using a General Area Detector Diffraction System (GADDS) from Bruker AXS, Inc., equipped with a two-dimensional (2D) detector.

The homogeneity of the films after pyrolysis was checked using a Leica DM 1750 M optical microscope. Atomic Force Microscopy (AFM) was used to provide high resolution, 3D information about the surface of the films through the available Agilent 5100 device.

Scanning Electron Microscopy (SEM) of the surfaces was carried out with a high resolution FEI Quanta 200 FEG system. Scanning Transmission Electron Microscopy (STEM) characterization was done using the probe corrected FEI Titan at 300kV and FEI Tecnai Osiris microscopes. High and Low angle Annular Dark Field (HAADF and LAADF) STEM together with Bright Field TEM (BFTEM) imaging and STEM Energy Dispersive X-ray Spectroscopy (EDX) mapping were performed.

The superconducting properties were characterized by DC magnetometry, using a Superconducting Quantum Interference Device magnetometer (SQUID) provided with a 9 T superconducting coil. The magnetic moment of the samples was obtained after subtracting the magnetic contribution from the metallic substrate [13]. AC susceptibility measurements were performed with a Quantum Design Physical Property Measurement System (PPMS) by using amplitudes between $\mu_0 H_{ac}$ =0.01–1.5 mT and dc-fields in the range of 0-9 T, at frequencies f =1111 Hz.

III. Structural Characterization

A. Characterization of the CGO buffer layer

The surface of the CGO cap layer observed by optical microscopy was very homogeneous. The surface topography was further characterized by AFM. Fig. 1(a) shows a topographic image, from which the CGO roughness was determined (rms = 1.7 nm). Following the methodology developed by Coll et al. [14], the percentage of the flat grains (planarity) from this cap layer was found to be 68% (Fig. 1(b)). The topographic image shows the presence of some outgrowths owing to the Pulsed Laser Deposition (PLD) process, whose height does not exceed 20-40 nm.

The structural characterization of the SuperOx tape was performed with a GADDS two dimensional detector (Fig. 2a). The two observed rings correspond to the polycrystalline, Hastelloy C276 metallic substrate, whereas the epitaxial spots correspond to the CGO(200), LMO(001)(002), MgO(200) and Y_2O_3(111) reflections. The width of the φ-scan of the CGO(111) reflexion was FWHM=7.4º, while that of the ω–scan at the CGO(200) reflection was 2.3º, indicating a good texturing of the CGO cap, better out-of-plane than in-plane.

B. Characterization of the CC tape

The structural and morphological properties of the LF-YBCO sample were investigated combining XRD, SEM and TEM. The microstructure of the YBCO film, crystallized at 790ºC under 200 ppm oxygen partial pressure on top of the SuperOx tape is shown in the SEM micrograph in Fig. 3. The YBCO film shows crack-free microstructure with c-axis oriented grains. Some pores and precipitates rich in copper can be appreciated on the surface.

The XRD pattern of the LF-YBCO sample is shown in Fig. 2(b). A good c-axis orientation of the YBCO layer is demonstrated by the strong intensity of the (00l) spots. The width of the φ-scan of the YBCO(103) reflexion was FWHM=3.9º, while that of the ω–scan at the YBCO(005) reflection was 1.5º, indicating a very good out-of-plane texture, better than in-plane. The improvement in the YBCO texture, sharper than for the CGO (φ-scan 7.4º, ω–scan 2.3º) could be a consequence of the epitaxial YBCO, nucleating preferentially on the grains of the cap layer having a lower misorientation and of the lamellar growth of these nuclei to the grain size much larger than that of the CGO.

STEM was used to characterize in more detail the microstructure of the LF-YBCO sample. Fig. 4 shows a low-resolution, cross-section image where the different layers of the CC architecture can be identified. Note that there is a reacted phase present at the interface between the cap CGO and the YBCO layers, identified as $BaCeO_3$ (BCO).

Further information on the composition of the set of buffer layers was obtained by EDX mapping. Fig. 5 shows the elemental concentration EDX maps obtained for Y, Cu, Ce, Ni, Al, Mg, La (Fig. 5(a)), together with the Ba and Ce maps (Fig. 5(b-c)), measured to elucidate the composition of the reactive phase between YBCO and CGO. From the compositional analysis, the set of buffer layers was confirmed to be Y_2O_3/MgO/LMO. On the surface of the metallic substrate, a passivation layer of about 40-50 nm, formed by Cr and Al, is observed. The major part of the initial 200 nm CGO remains unreacted but a reactive phase (BCO) of about 30-40 nm thick can also be identified in Fig. 5(b-c).

A detail of this reactive layer BCO layer sandwiched in between the CGO and YBCO layers is shown in the TEM image of Fig. 6(a). YBCO grows c-axis oriented on top of BCO, and thus the presence of this partial reactivity does not degrade the superconducting properties.

A deeper characterization of the morphology of the sample was done using HAADF-STEM imaging. The approximate thickness of the YBCO grains observed from various images was found to be ~0.5-1 μm. A high resolution image of the YBCO matrix is shown in Fig. 6(b). The orange arrows indicate high number of short $Y_2Ba_4Cu_8O_{16}$ (Y248) intergrowths. Some triple Cu chains are incorporated in these Y248 phases, resulting in local Y125 intergrowths.

IV. Magnetic Characterization

The magnetic hysteresis loops measured for the LF-YBCO sample for a maximum applied field of $\mu_0 H_m$=5 T at 5, 50 and 77 K after subtracting the substrate contribution is shown in Fig 7(a). The $M(H)$ cycles exhibit a maximum on the reverse branch of the magnetization at positive applied magnetic fields (Fig. 7(a), inset), a feature associated to granularity [15], *vide infra*. The percolating, inter-grain critical current density field-dependence is determined from these saturated loops applying Bean's approximation for a thin disc, $J_c^{GB}(H)=3M(H)/R$, where R is the effective radius of the sample (Fig. 7(b). The LF-YBCO reaches self-field critical current density values of J_c^{GB}~15.9 MA/cm^2 (5 K), ~6.06 MA/cm^2 (50 K) and ~1.23 MA/cm^2 (77 K). This corresponds to a current per centimeter width of I_c=58.4 A/cm-width.

For the sake of comparison, the percolating critical current at the same temperatures of the previously reported ABAD CC sample is also shown in Fig. 7(b). The values of J_c^{GB} reached in self-field by the LF-YBCO sample are slightly above those of TFA-YBCO. The intergranular $J_c^{GB}(H)$ dependence of the two samples is qualitatively similar to that reported for other CCs [13]. It is observed that while the plateau at low fields and crossover to the J_c^{GB}~$H^{-0.5}$ region is similar for the two samples, the decrease of $J_c^{GB}(H)$ occurs at smaller fields for the LF-YBCO, reflecting a somewhat smaller irreversibility line. This might be related to the presence of a large density of short stacking faults observed by STEM in Fig. 6(b), which have been reported to break the length of twin boundaries, decreasing the vortex pinning efficiency at high fields [16].

In order to further characterize the granularity of the LF-YBCO sample, we applied the method developed by A. Palau *et al*. [15] to simultaneously determine the grain size $\langle 2a \rangle$, intergranular J_c^{GB} and intragranular J_c^{G} critical currents from the measurement of $M(H)$ minor loops, showing a progressive saturation of the granularity peak (Fig. 8a).

From the experimentally determined values for the saturation field of the peak, $\mu_0 H_{peak}^{sat}$=422 mT, and the maximum field at which the remanent magnetization saturates, $\mu_0 H_m(M_{rem}^{sat})$=292 mT (Fig. 8b), we estimated a grain diameter of $\langle 2a \rangle \approx 0.80 \pm 0.05$ μm, compatible with the grain size found by TEM (~0.5-1 μm). This grain size is within the values reported for IBAD samples, $\langle 2a \rangle \approx$0.5-5 μm [17]. Furthermore, the intragrain critical current density determined was J_c^{G}(5K)=49±2 MA/cm^2 and the inter-to-intragrain critical current density ratio was J_c^{GB}/J_c^{G}=0.3. Comparing the granular characteristics of the LF-YBCO tape and previously reported TFA-YBCO tape (Table 1), the following conclusions can be drawn. First, it is observed that that the deposition of YBCO on the SuperOx tape results in a smaller size of the grains, something not surprising since the two utilized substrates are different. Besides, a high J_c^{G} is attained for LF-YBCO sample, even larger than that of TFA_YBCO. However, the inter-to-intragrain current density ratio determined at 5 K is smaller for the LF-YBCO (J_c^{GB}/J_c^{G}=0.32) than for the TFA-YBCO (J_c^{GB}/J_c^{G}=0.46). The diminished intergranular performance may be due to different degrees of optimized texture qualities in both films [18].

AC measurements were performed in order to investigate the CC homogeneity. Fig. 9 shows the measured temperature dependence of the real and imaginary components of the ac susceptibility, χ', $\chi''(T)$ in self-field at different ac fields at constant frequency f. The critical temperature, measured from the transition of the $\chi'(T)$ curve to cero at $\mu_0 H_{ac}$=0.1 mT was T_c=88.5 K, with a narrow transition width, defined as $\Delta T = T_c - T'$(at $0.95\chi'/\chi_0$), of ΔT=2.3 K. T_c is slightly smaller than values typically found in thin-films and CCs grown by the TFA CSD method, something which may be explained by the previous mentioned presence of C in the GBs. Fig. 9 shows that the $\chi''(T)$ curves measured for the LF-YBCO sample presents a single peak, similar to a non-granular film, i.e., flux penetrates from the surface to the centre of the sample through the homogeneous network of low angle GBs following the critical state [19].

The temperature dependence of the intergrain critical current density was determined from the peaks of the $\chi''(T)$ curves measured at different AC field amplitudes, according to: $J_c^{GB}(T_{peak})=2H_{ac}/1.94t$. The AC determined $J_c^{GB}(T)$ curve corresponding to the main, homogeneous network of low-angle GBs has been extrapolated to the DC data obtained at 5, 50, 77 K, considering that SQUID measurements are only sensitive to the highest J_c percolative domain. As shown in Fig. 10, the temperature dependence of the percolative critical current is very similar to that earlier found for the TFA-YBCO sample.

V. Conclusions

We have fabricated a new CC architecture $YBa_2Cu_3O_7$/CGO/LMO/MgO/Y_2O_3/Al_2O_3/Hastelloy based on the low-fluorine chemical-solution route using reel-to-reel Inkjet printing deposition. The total thickness of the YBCO film was 475±25 nm after a 5-multi-deposition process. A good texture of the resulting film was achieved utilizing a very thin 30 nm IBAD-MgO layer. A magnetically homogeneous YBCO films was obtained, exhibiting a self-field percolative critical current density of J_c^{GB}=1.23 MA/cm^2 at 77 K (i.e. an I_c=58.4 A/cm-width). Scaling of this architecture to 10 m long tapes at Oxolutia is foreseen in the close future.

References

[1] R. Horst and K. H. Peter, *100 Years of Superconductivity (London: Chapman and Hall)*. 2011.

[2] "European development of Superconducting tapes: integrating novel materials and architectures into cost effective processes for power applications and magnets" EUROTAPES, Grant Agreement FP7-NMP-Large-2011-280432.[Online]. Available: www.eurotapes.eu

[3] M. Vilardell, X. Granados, S. Ricart, I. Van Driessche, A. Palau, T. Puig, and X. Obradors, "Flexible manufacturing of functional ceramic coatings by inkjet printing," *Thin Solid Films*, vol. 548, pp. 489–497, 2013.

[4] E. Bartolomé, V. R. Vlad, a Calleja, M. Aklalouch, R. Guzmán, J. Arbiol, X. Granados, a Palau, X. Obradors, T. Puig, and a Usoskin, "Magnetic and structural characterization of inkjet-printed TFA YBa 2 Cu 3 O 7− x / MOD CZO/ ABAD YSZ/SS coated conductors," *Supercond. Sci. Technol.*, vol. 26, p. 125004, 2013.

[5] I. Van Driessche, J. Feys, S. C. Hopkins, P. Lommens, X. Granados, B. A. Glowacki, S. Ricart, B. Holzapfel, M. Vilardell, A. Kirchner, and M. B. Backer, "Chemical solution deposition using ink-jet printing for YBCO coated conductors," *Supercond. Sci. Technol.*, vol. 25, p. 065017, 2012.

[6] S. C. Hopkins, D. Joseph, T. B. Mitchell-Williams, A. Calleja, V. R. Vlad, M. Vilardell, S. Ricart, X. Granados, T. Puig, X. Obradors, A. Usoskin, M. Falter, M. Bäcker, and B. A. Glowacki, "Inkjet printing of multifilamentary YBCO for low AC loss coated conductors," *J. Phys. Conf. Ser.*, vol. 507, no. 2, p. 022010, 2014.

[7] A. Usoskin and L. Kirchhoff, "In-Plane Texturing of Buffer Layers by Alternating Beam Assisted Deposition: Large Area and Small Area Applications," *Mater. Res. Soc. Symp. Proc.*, vol. 1150, pp. 117–122, 2009.

[8] S. C. Hopkins, T. B. Mitchell-Williams, D. R. Vanden Bussche, A. Calleja, V. R. Vlad, M. Vilardell, X. Granados, T. Puig, X. Obradors, A. Usoskin, M. Soloviov, M. Vojenciak, F. Gomory, I. Van Driessche, M. Backer, and B. A. Glowacki, "Low AC Loss Inkjet-Printed Multifilamentary YBCO Coated Conductors," *IEEE Trans. Appl. Supercond.*, vol. 26, no. 3, Apr. 2016.

[9] V. Matias, B. J. Gibbons, A. T. Findikoglu, P. C. Dowden, J. Sullard, and J. Y. Coulter, "Continuous fabrication of IBAD-MgO based coated conductors," *IEEE Transactions on Applied Superconductivity*, vol. 15, no. 2. pp. 2735–2738, 2005.

[10] S. Lee, V. Petrykin, A. Molodyk, S. Samoilenkov, A. Kaul, A. Vavilov, V. Vysotsky, and S. Fetisov, "Development and production of second generation high Tc superconducting tapes at SuperOx and first tests of model cables," *Supercond. Sci. Technol.*, vol. 27, no. 4, p. 44022, 2014.

[11] X. Palmer, C. Pop, H. Eloussifi, B. Villarejo, P. Roura, J. Farjas, A. Calleja, A. Palau, X. Obradors, T. Puig, and S. Ricart, "Solution design for low-fluorine trifluoroacetate route to YBa2Cu3O7 films," *Supercond. Sci. Technol.*, vol. 29, no. 2, p. 24002, 2016.

[12] X. Obradors, T. Puig, S. Ricart, M. Coll, J. Gazquez, and X. Granados, "Growth, nanostructure and vortex pinning in superconducting YBa2Cu3O7 thin films based on trifluoroacetate solutions," *Supercond. Sci. Technol.*, vol. 25, pp. 123001, doi:10.1088/0953–2048/25/12/123001, 2012.

[13] A. Palau, T. Puig, X. Obradors, and C. Jooss, "Simultaneous determination of grain and grain-boundary critical currents in YBa2Cu3O7-coated conductors by magnetic measurements," *Phys. Rev. B*, vol. 75, pp. 1–12, 2007.

[14] M. Coll, A. Pomar, T. Puig, and X. Obradors, "Atomically Flat Surface: The Key Issue for Solution-Derived Epitaxial Multilayers," *Appl. Phys. Express*, vol. 1, no. 12, pp. 121701–121703, 2008.

[15] A. Palau, T. Puig, X. Obradors, E. Pardo, C. Navau, A. Sanchez, A. Usoskin, H. C. Freyhardt, L. Fernández, B. Holzapfel, and R. Feenstra, "Simultaneous inductive determination of grain and intergrain critical current densities of YBa2Cu3O7-x coated conductors," *Appl. Phys. Lett.*, vol. 84, no. 2, pp. 230–232, 2004.

[16] V. Rouco, A. Palau, R. Guzman, J. Gazquez, M. Coll, X. Obradors, and T. Puig, "Role of twin boundaries on vortex pinning of CSD YBCO nanocomposites," *Supercond. Sci. Technol.*, vol. 27, no. 12, p. 125009, 2014.

[17] A. Palau, T. Puig, J. Gutierrez, X. Obradors, and F. de la Cruz, "Pinning regimes of grain boundary vortices in YBa2Cu3O7-x coated conductors," *Phys. Rev. B*, vol. 73, no. 13, p. 132508, Apr. 2006.

[18] P. Cayado, B. Mundet, H. Eloussifi, F. Vallés, M. Coll, S. Ricart, J. Gázquez, A. Palau, P. Roura, J. Farjas, T. Puig, and X. Obradors, "Epitaxial superconducting GdBa2Cu3O7-d/Gd2O3 nanocomposite thin films from advanced low-fluorine solutions," *Supercond. Sci. Technol.*, vol. 30, p. 125010, 2017.

[19] A. Palau, T. Puig, and X. Obradors, “Grain and grain boundary vortex dynamics in YBa2Cu3O7-δ coated conductor by ac susceptibility,” *J. Appl. Phys.*, vol. 102, no. 7, p. 73911, 2007.

FIGURES AND TABLES:

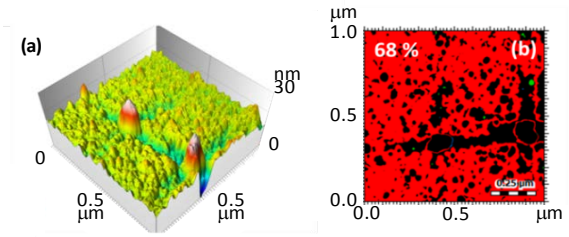

Fig. 1 (a) topographic 1 µm x 1 µm 3D-AFM images of the CGO top layer from the SuperOx tape; (b) binarization of the topographic image, where the flat cerium grains are shown in red.

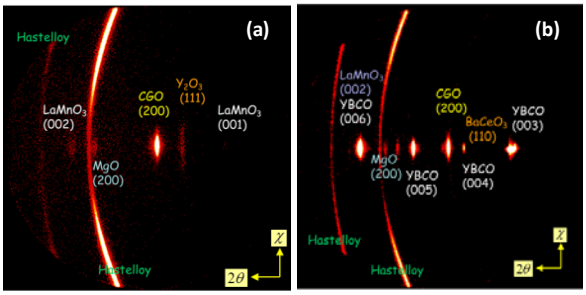

Fig. 2 2D XRD pattern of (a) SuperOx tape; (a) the LF-YBCO sample.

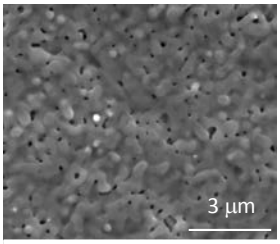

Fig. 3 High resolution SEM micrograph of the LF-YBCO sample.

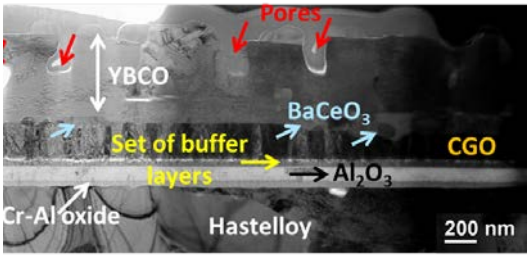

Fig. 4 Cross-sectional TEM image showing the CC architecture.

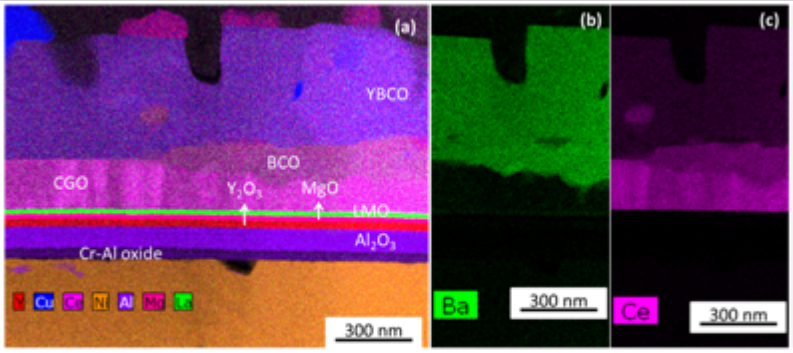

Fig. 5 EDX maps of the whole architecture (a); maps for Ba (b) and Ce (c).

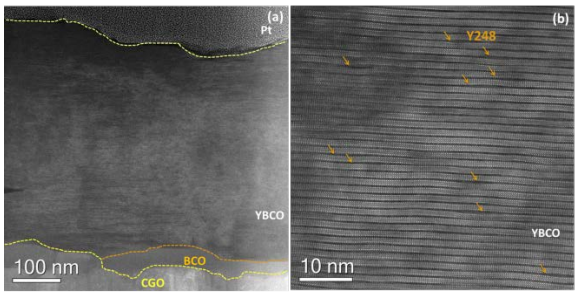

Fig. 6 (a) TEM image of the interface of BCO with YBCO; (b) high resolution HAADF-STEM Z-contrast image showing the stacking defects.

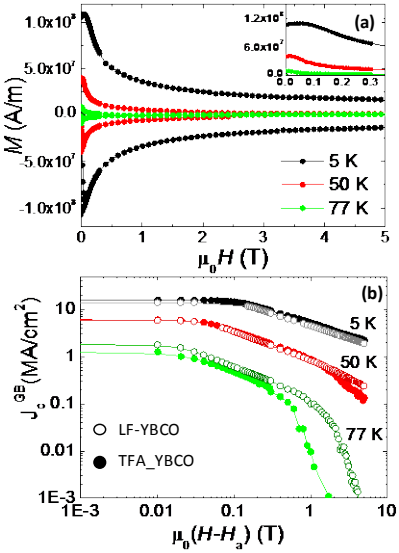

Fig.7 a) Hysteresis loops for the LF-YBCO sample at T=5, 50 and 77 K. Inset: granularity peaks in the reverse branch of the magnetization; b) $J_c^{GB}(H)$ of the same sample and TFA-YBCO CC [4] for comparison.

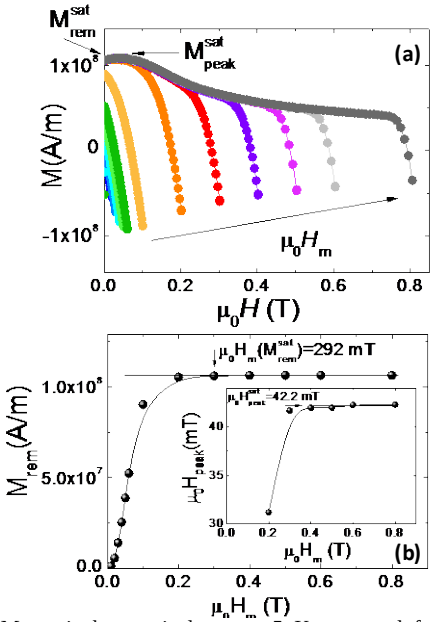

Fig.8 (a) Magnetic hysteresis loops at 5 K measured for the LF-YBCO sample for increasing $\mu_0 H_m$ from 0 - 0.8 T; (b) Evolution of the remanent magnetization and (inset) of the peak position H_{peak} as a function of the maximum applied field H_m at 5 K.

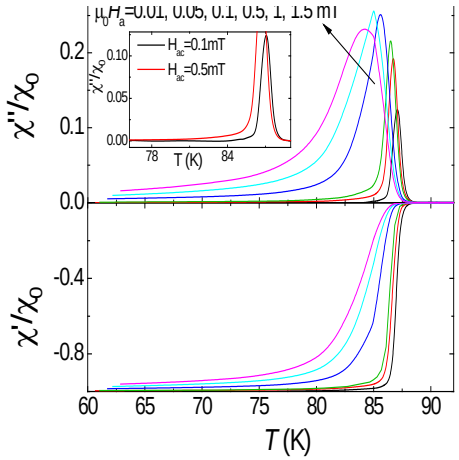

Fig. 9 (a) $\chi'/\chi_0(T)$ and $\chi''/\chi_0(T)$, measured in self-field, at f=1111 Hz and different AC fields $\mu_0 H_{ac}$ for LF-YBCO. Top (inset): zoom of $\chi''/\chi_0(T)$ showing the absence of residual peaks.

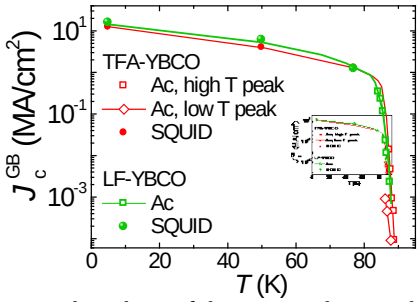

Fig. 10 Temperature dependence of the intergranular critical current density determined from the T_{peak} position of the χ'' peaks and from SQUID measurements for LF-YBCO and TFA-YBCO sample [4].

TABLE I

GRANULARITY PARAMETERS FOR LF-YBCO AND TFA-YBCO

	LF-YBCO (0.475μm)		TFA-YBCO (0.9μm)	
	5 K	77K	5K	77 K
$\mu_0 H_{peak}^{sat}$ (mT)	42.2		68.4	
$\mu_0 H_m(M_{rem}^{sat})$ (mT)	292		360	
$<2a>$ (μm)	0.8±0.5		2.2±0.5	
J_c^G (MA/cm^2)	49±5		27±5	
J_c^{GB} (MA/cm^2)	15.9	1.23	12.5	1.3